



**HAL**  
open science

## Rationally designed hyaluronic acid-based nano-complexes for pentamidine delivery

Flavia Carton, Yves Chevalier, Letizia Nicoletti, Malgorzata Tarnowska, Barbara Stella, Silvia Arpicco, Manuela Malatesta, Lars Petter Jordheim, Stephanie Briancon, Giovanna Lollo

### ► To cite this version:

Flavia Carton, Yves Chevalier, Letizia Nicoletti, Malgorzata Tarnowska, Barbara Stella, et al.. Rationally designed hyaluronic acid-based nano-complexes for pentamidine delivery. *International Journal of Pharmaceutics*, 2019, 568, pp.118526. 10.1016/j.ijpharm.2019.118526 . hal-02841561

**HAL Id: hal-02841561**

**<https://hal.science/hal-02841561>**

Submitted on 20 Jul 2022

**HAL** is a multi-disciplinary open access archive for the deposit and dissemination of scientific research documents, whether they are published or not. The documents may come from teaching and research institutions in France or abroad, or from public or private research centers.

L'archive ouverte pluridisciplinaire **HAL**, est destinée au dépôt et à la diffusion de documents scientifiques de niveau recherche, publiés ou non, émanant des établissements d'enseignement et de recherche français ou étrangers, des laboratoires publics ou privés.



Distributed under a Creative Commons Attribution - NonCommercial 4.0 International License

# Rationally designed hyaluronic acid-based nano-complexes for pentamidine delivery

3

4 *Flavia Carton*<sup>1,2</sup>, *Yves Chevalier*<sup>1</sup>, *Letizia Nicoletti*<sup>1,3</sup>, *Małgorzata Tarnowska*<sup>1</sup>, *Barbara Stella*<sup>3</sup>,  
5 *Silvia Arpicco*<sup>3</sup>, *Manuela Malatesta*<sup>2</sup>, *Lars Petter Jordheim*<sup>4</sup>, *Stéphanie Briançon*<sup>1</sup>, and *Giovanna*  
6 *Lollo*<sup>1\*</sup>

7 <sup>1</sup>University of Lyon, Université Claude Bernard Lyon 1, CNRS, LAGEPP UMR 5007, 43 bd 11  
8 Novembre 1918, 69622, Villeurbanne, France.

9 <sup>2</sup>Department of Neurosciences, Biomedicine and Movement Sciences, Anatomy and Histology  
10 Section, University of Verona, Strada le Grazie 8, Verona, Italy.

11 <sup>3</sup>Department of Drug Science and Technology, University of Torino, Via P. Giuria 9, Torino, Italy.

12 <sup>4</sup>University of Lyon, Université Claude Bernard Lyon 1, INSERM 1052, CNRS 5286, Centre Léon  
13 Bérard, Centre de Recherche en Cancérologie de Lyon, 69008 Lyon, France.

14

15 **Keywords:** hyaluronic acid, polyarginine, pentamidine, biomaterials, drug delivery systems;

16 **\*Corresponding Author**

17 **\*E-mail:** [giovanna.lollo@univ-lyon1.fr](mailto:giovanna.lollo@univ-lyon1.fr)

18

## 19 **Abstract**

20 Nanoparticles of polymeric complexes made of hyaluronic acid and polyarginine were investigated  
21 for the encapsulation of the cationic hydrophilic drug pentamidine isethionate. The interaction  
22 between the anionic hyaluronic acid and the cationic pentamidine and the formation of  
23 polyelectrolyte complexes of them were firstly studied. Then, nanoparticles made of mixed  
24 hyaluronic acid / polyarginine loaded with pentamidine were developed as drug delivery systems. A  
25 monodisperse population of negatively charged pentamidine-loaded nanoparticles allowed high  
26 encapsulation rates of pentamidine (80%). Such high encapsulation efficiency coming from ion  
27 exchange was confirmed by measurements of the counterion isethionate released from pentamidine  
28 during nanoparticles formation. Besides, freeze-dried pentamidine-loaded nanoparticles kept their  
29 integrity after their reconstitution in water. *In vitro* studies on human lung (A549) and breast  
30 (MDA-MB-231) cancer cell lines showed that pentamidine-loaded nanoparticles were more  
31 cytotoxic in comparison to the free drug, suggesting an enhanced internalization of encapsulated  
32 drug by cancer cells.

33

## 34 **1. Introduction**

35 Delivery of hydrophilic drugs is a challenge owing to their difficult crossing through cells walls that  
36 limits their therapeutic activity. Encapsulation is often required in order to enhance drug  
37 bioavailability. In case of ionic drugs, complexation with polyelectrolytes of opposite charge is a  
38 suitable methodology as it has been extensively studied for transfection of DNA and siRNA<sup>1,2</sup>.  
39 Upon formation of a charge-stoichiometric complex, the neutral species may undergo precipitation  
40 as nanoparticles, resulting in drug encapsulation inside a nanocarrier. Electrostatic interaction is one  
41 of the driving forces for such complexation. However, electrostatic binding often occurs by an ion  
42 exchange process such that the overall charge balance is null. Non-electrostatic interactions also  
43 matter, so that each system deserves a specific investigation aiming at better mastery over the  
44 encapsulation process.

45 Over the last decades, the development of pharmaceutical nanocarriers based on natural  
46 polysaccharides aroused a growing interest in drug delivery technologies based on ionic  
47 complexation<sup>3</sup>. Natural polysaccharides have interesting properties as biocompatibility,  
48 biodegradability and low toxicity suitable for biomedical applications<sup>4-6</sup>. Besides, they bear a large  
49 variety of reactive groups, a wide range of molar masses ( $M_w$ ), varying chemical compositions and  
50 origins, which make them a versatile biomaterial for the preparation of nanometric carriers<sup>7</sup>.

51 Among the different natural polysaccharides, hyaluronic acid (HA) has been widely used in the  
52 pharmaceutical field because of its interesting physicochemical and biological properties<sup>8,9</sup>. HA  
53 belongs to the class of anionic glycosaminoglycans (GAGs) formed by several identical subunits  
54 (D-glucuronic acid and N-acetyl-D-glucosamine disaccharide) bound together by  $\beta$ -1,4 and  $\beta$ -1,3  
55 glycosidic bonds<sup>10,11</sup>. HA is an important component of the extracellular matrix (ECM) highly  
56 distributed throughout connective, epithelial, and neural tissues in which plays essential  
57 physiological roles<sup>8</sup>. HA backbone itself is endowed with targeting moieties that specifically  
58 recognize and interact with different cell surface proteins like stabilin-2, RHAMM, lymphatic  
59 vessel endothelial hyaluronan receptor 1 (LYVE-1), and CD44. Also, low molar mass HA regulates  
60 Toll Like Receptor (TRL). Among all these receptors, CD44 represents the most studied HA-  
61 receptor in inflammation and tumor pathologies<sup>9,12,13</sup>.

62 Therefore, specific targeting of these receptors has been exploited as an effective strategy for  
63 increasing accumulation of associated drug at the target site<sup>14,15</sup>. In addition, HA bears a carboxylic  
64 group in each glucuronic unit ( $pK_a$  3-4) which provides an acidic polyelectrolyte character enabling  
65 interactions with cationic polymers or molecules possessing appropriate basic groups for formation  
66 of complexes<sup>16</sup>.

67 So far, exploitation of HA properties to polymeric conjugates, liposomes, microparticles, and  
68 nanoparticles have been attempted. Such dosage forms are generally obtained through formation of  
69 self-assembling micelles, chemical conjugation via cross-linking approaches or ionic gelation<sup>16-19</sup>.  
70 Among these techniques, polyelectrolyte complexation represents the most widely used method to

71 tailor HA-based drug delivery systems, because of the mild processing conditions, absence of  
72 organic solvents and wide range of cationic polymers undergoing interactions with HA<sup>20</sup>. Several  
73 previous works disclosed instances showing the ability of HA-based polyelectrolyte nanostructures  
74 to associate active compounds such as genetic materials or positively charged drugs<sup>9</sup>. Contreras-  
75 Ruiz et al. described nanoparticles made of HA complexed with chitosan (CS) oligomers for pDNA  
76 delivery. HA-CS complexes entered cells and yielded significant transfection of pDNA into the  
77 corneal and conjunctival cells<sup>21</sup>. Recently, a novel ionic metal complex based on HA and an  
78 oxaliplatin derivative, dichloro(1,2-diaminocyclohexane)platinum(II) (DACHPt), has been  
79 patented. Compared to the DACHPt aqueous solution injected intravenously, DACHPt-loaded  
80 nano-complexes protected the associated drug from enzymatic degradation, thereby enhancing  
81 plasmatic concentration while lowering drug elimination rate<sup>22</sup>. Also, Battistini et al. reported a  
82 doxorubicin-HA ionic complex as a tumor targeting drug delivery system. *In vitro* studies on tumor  
83 cells overexpressing CD44 receptors demonstrated the improved internalization of the complexes in  
84 comparison to the free drug<sup>14</sup>.

85 Based on this background information, the present work deals with an extensive physicochemical  
86 characterization of polyelectrolyte complexes (PECs) made of HA and a cationic molecule,  
87 pentamidine isethionate (PTM) as a model drug. PTM is well known for its antiprotozoal,  
88 antifungal and anticancer activity<sup>23,24</sup>. It is a water-soluble molecule with two terminal amidine  
89 groups, protonated in a wide pH range ( $pK_a = 12-13$ ) including physiological/neutral conditions. To  
90 stabilize PTM-HA PECs and maximize the amount of associated PTM, polyarginine (PArg) was  
91 used to crosslink HA and form nanoparticles (NPs). PArg is a biocompatible cationic  
92 poly(aminoacid) belonging to the cell-penetrating peptide polymers able to improve intracellular  
93 delivery of therapeutic agents<sup>25</sup>. At neutral pH, the amine groups of PArg are protonated and  
94 interact with carboxylic moieties of HA, leading to the formation of NPs. Also, polyion complexes  
95 made of HA and protamine, have been described and developed for the encapsulation of different  
96 active compounds<sup>26,27</sup>. In the current work, the formation of PECs made of HA and PTM and NPs

97 **made of HA and PArg were investigated by** studying size and zeta potential of NPs and quantifying  
98 the amount of isethionate, the PTM counterion, released during the formation process while varying  
99 the relative concentrations of the PECs-forming components. Lyophilization studies were also  
100 carried out in order to ensure preservation of pentamidine-loaded nanoparticles (PTM-loaded NPs)  
101 as a dry form upon long-term storage. The morphology of the formed particles was analyzed by  
102 transmission electron microscopy (TEM) and cryogenic-transmission electron microscopy (Cryo-  
103 TEM). Finally, *in vitro* studies were performed on lung and breast human cell lines (A549 and  
104 MDA–MB 231) to assess the anticancer activity of encapsulated PTM.

105

## 106 **2. Experimental section**

### 107 **2.1. Materials**

108 Sodium hyaluronate (HA) (weight-average molar mass,  $M_w = 3.9 \times 10^4 \text{ g} \cdot \text{mol}^{-1}$ ) was purchased from  
109 LifeCore<sup>®</sup> Biomedical (Chaska, Minnesota, USA). Poly (L-arginine hydrochloride) (PArg) (weight-  
110 average molar mass,  $M_w = 5.8 \times 10^3 \text{ g} \cdot \text{mol}^{-1}$ ) was purchased from Alamanda<sup>®</sup> Polymers (Huntsville,  
111 Alabama, USA) and pentamidine isethionate (PTM) (molar mass,  $M_{\text{mol}} = 592.679 \text{ g} \cdot \text{mol}^{-1}$ ) from  
112 Sigma-Aldrich<sup>®</sup> (St Quentin-Fallavier, France). Milli-Q water was obtained using a milli-Q  
113 Academic System (Merck Millipore<sup>®</sup>, St Quentin-Fallavier, France). Sodium silicotungstate used  
114 for staining in TEM was supplied from Agar Scientific (Parsonage Lane, Stansted, UK). Dulbecco's  
115 Modified Eagle Medium (DMEM) without glucose, glutamine, phenol red and sodium pyruvate  
116 was bought from Gibco<sup>®</sup> (Thermo Fisher Scientific<sup>®</sup>, Waltham, Massachusetts, USA) and used to  
117 evaluate the stability in physiological medium. Human lung carcinoma cells (A549) and human  
118 breast adenocarcinoma cells (MDA-MB-231) were from ATCC and grown in complete Dulbecco's  
119 Modified Eagle Medium (DMEM) supplemented with 10% fetal bovine serum (Thermo Fisher  
120 Scientific<sup>®</sup>), 100 U/mL penicillin (Thermo Fisher Scientific<sup>®</sup>), 100 mg·mL<sup>-1</sup> streptomycin (Thermo  
121 Fisher Scientific<sup>®</sup>) and 1% L-glutamine (Life Technologies<sup>®</sup>). 3-(4,5-dimethylthiazol-2-yl)-2,5-

122 diphenyltetrazolium bromide (MTT) was purchased from Sigma-Aldrich® (St Quentin-Fallavier,  
123 France).

124

## 125 **2.2. Solubility study of pentamidine**

126 Saturated solutions of PTM at different pH (pH 7.4, 9, 10, 12) and in phosphate buffer saline (PBS,  
127 pH 7.4) were prepared. The solutions were stirred for 2 h at room temperature and left overnight to  
128 reach equilibrium. Then, all samples were centrifuged (62,000 g, 30 min, 20 °C) and the  
129 supernatant was analyzed for PTM by measuring its UV absorbance at 270 nm (UV-1280,  
130 Shimadzu, Marne-la-Vallée, France).

131

## 132 **2.3. Preparation of pentamidine-hyaluronic acid polyelectrolyte complexes**

133 Pentamidine-hyaluronic acid polyelectrolyte complexes (PTM-HA PECs) were prepared by mixing  
134 aqueous solutions of PTM and HA at different PTM/HA mole ratios ranging between 0.2 and 2.4.  
135 Seven different PTM-HA PECs were obtained by adding 0.5 mL of HA aqueous solution  
136 ( $2.5 \text{ mg}\cdot\text{mL}^{-1}$ ) into 0.5 mL of PTM aqueous solution of concentrations ranging from 0.6 to  
137  $9 \text{ mg}\cdot\text{mL}^{-1}$ . Size, polydispersity index, electrophoretic mobility and pH of PECs were studied.

138

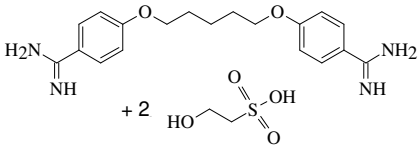
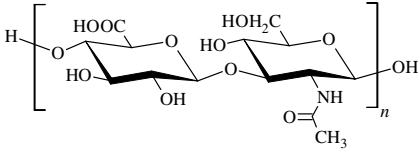
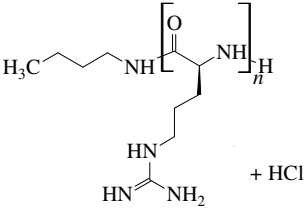
## 139 **2.4. Preparation of blank and pentamidine-loaded nanoparticles**

140 Blank nanoparticles (HA-PArg NPs) were prepared by polyelectrolyte complexation using a similar  
141 methodology of ionic gelation<sup>20</sup>. Briefly, 0.5 mL of an anionic HA solution at different  
142 concentrations ranging from 1.25 to  $5.00 \text{ mg}\cdot\text{mL}^{-1}$  were added to an equal volume of solution  
143 containing cationic polyarginine (PArg) ( $0.27 \text{ mg}\cdot\text{mL}^{-1}$ ). Nine different formulations with HA/PArg  
144 mole ratio between 0.82 to 8.25 were prepared.

145 Pentamidine-loaded nanoparticles (PTM-loaded NPs) were obtained by mixing 0.5 mL of aqueous  
146 solution of PTM at concentrations ranging from  $0.50$  to  $0.17 \text{ mg}\cdot\text{mL}^{-1}$  and 0.5 mL of cationic PArg  
147 solution at  $0.18 \text{ mg}\cdot\text{mL}^{-1}$ . This premix was left under agitation during 10 min, and 0.5 mL of HA

148 solution of concentrations ranging from 0.83 to 3.3 mg·mL<sup>-1</sup> were added. The mole ratio between  
 149 HA (negatively charged) and PArg plus PTM (both positively charged) was ranging between 1.13  
 150 and 4.51. HA-PArg NPs and PTM-loaded NPs were characterized in terms of pH, size,  
 151 polydispersity index, zeta potential and encapsulation efficiency. The main characteristics of all the  
 152 compounds used to obtain PECs and NPs are listed in Table 1.

153  
 154 **Table 1.** Chemical characteristics of the compounds used to obtain polyelectrolyte complexes and  
 155 nanoparticles. The molar masses given for polymers are that of their repeat unit.

Compound	Molecular Formula	Molecular structure	pKa	M <sub>w</sub> (g·mol <sup>-1</sup> )
Pentamidine isethionate	C <sub>23</sub> H <sub>36</sub> N <sub>4</sub> O <sub>10</sub> S <sub>2</sub>		12.13	592.7
Sodium Hyaluronate	(C <sub>14</sub> H <sub>20</sub> NO <sub>11</sub> Na) <sub>n</sub>		2.87	3.9·10 <sup>4</sup>
Poly(L-arginine hydrochloride)	(C <sub>6</sub> H <sub>14</sub> N <sub>4</sub> O <sub>2</sub> ) <sub>n</sub>		12.42	5.8·10 <sup>3</sup>

156

## 157 2.5. Physicochemical characterization of polyelectrolyte complexes, blank and 158 pentamidine-loaded nanoparticles

159 Size distribution and surface potential of the prepared particles (PECs and NPs) were analyzed  
 160 using a Malvern Zetasizer<sup>®</sup> (model Nano ZS, Malvern Panalytical, Malvern, UK). Particle size  
 161 distributions were determined by Dynamic Light Scattering (DLS) of samples diluted with milli-Q



162 water. Analyses were carried out at 25 °C with a scattering angle of 173°. Particle size distribution  
163 was determined using the cumulants method that provides the *z*-average diameter and the  
164 polydispersity index (*Pdl*). The zeta potential ( $\zeta$ ) was determined from the electrophoretic mobility  
165 ( $u_E$ ) (Equation 1). For all measurements, samples were diluted in milli-Q water and placed in a U-  
166 shaped fold capillary cell (DTS1070) made of polystyrene and containing two electrodes of gold-  
167 plated beryllium/copper (Malvern).  $\zeta$  potential was calculated according to the Henry Equation<sup>28</sup>  
168 under the Smoluchowski approximation of the Henry factor  $f(\kappa a)$ :

$$169 \quad u_E = \frac{2}{3} \frac{\epsilon_0 \epsilon \zeta}{\eta} f(\kappa a) \quad (1)$$

170 where  $\eta$  is the viscosity of water ( $\eta = 0.887$  mPa·s at 25°C),  $\kappa$  is the inverse Debye length,  $a$  is the  
171 radius of particles, and  $f(\kappa a) = 3/2$ .

172 Turbidity of PECs was monitored by absorbance measurements at 600 nm using an UV  
173 spectrometer (UV-1280 from Shimadzu, Marne-la-Vallée, France) equipped with a cuvette with an  
174 optical path of 10 mm. The turbidity ( $\tau$ ) was calculated from the absorbance (*Abs*) reading as  $\tau = \ln$   
175 (10) *Abs* = 2.3 *Abs*.

176

## 177 **2.6. Ion-exchange chromatography**

178 Isethionate ions released due to association of positively charged PTM to negatively charged HA  
179 were quantified using ion exchange chromatography (IC) (930 Compact IC Flex, Metrohm,  
180 Switzerland) equipped with a chemical suppressor and conductivity detection. PTM-loaded NPs  
181 were centrifuged (7,000 g, 30 min, 25 °C) using Amicon<sup>®</sup> filter (Amicon Ultra-0.5, 30,000 NMWL,  
182 Millipore, Darmstadt, Germany), supernatants were recovered and injected into the IC. The  
183 analyses were conducted using Metrosep a Supp 5 250/4.0 column with an adequate pre-column at  
184 a temperature of 30°C. For the detection of anions, the mobile phase was 8 mmol·L<sup>-1</sup> solution of  
185 Na<sub>2</sub>CO<sub>3</sub> (Fischer Scientific, Illkirch, France) prepared in ultrapure water (resistivity > 18 MΩ·cm),  
186 filtered at 0.45 μm and degassed in an ultrasonic bath prior to use. The flow rate was 0.7 mL·min<sup>-1</sup>.

187 Such conditions ensured linearity of calibration curve in a range from 0.005 to 5 mmol·L<sup>-1</sup> of  
188 isethionate concentration.

189

## 190 **2.7. Morphology of blank and loaded nanoparticles using transmission and cryogenic** 191 **electron microscopy**

192 Transmission electron microscopy (TEM) was performed with a Philips CM120 microscope at  
193 “Centre Technologique des Microstructures” (CTμ) at the University of Lyon 1 (Villeurbanne,  
194 France). A small drop of suspension (5 μL) was deposited on a carbon/formvar microscope grid  
195 (Delta Microscopies, Saint-Ybars, France), stained with a 1% w/w sodium silicotungstate aqueous  
196 solution, and slowly dried in open air. The dry samples were observed by TEM under 120 kV  
197 acceleration voltage.

198 Regarding cryogenic-transmission electron microscopy (Cryo-TEM), diluted samples of HA-PArg  
199 NPs and PTM-loaded NPs were dropped onto 300 mesh holey carbon films (Quantifoil R2/1) and  
200 quench-frozen in liquid ethane using a cryo-plunge workstation (made at Laboratoire de Physique  
201 des Solides-LPS Orsay, France). The specimens were then mounted on a precooled Gatan 626  
202 specimen holder, transferred in the microscope (Phillips CM120) and observed at an accelerating  
203 voltage of 120 kV.

204

## 205 **2.8. Association efficiency and loading capacity of pentamidine into nanoparticles**

206 The association efficiency (AE) of PTM into loaded NPs **was determined using an indirect method**  
207 by measurements of the concentration of free PTM in the aqueous phase. PTM-loaded NPs were  
208 centrifuged (**7,000 g**, 30 min, 25°C) using Amicon<sup>®</sup> filter (Amicon Ultra-0.5, 30.000 NMWL,  
209 Merck Millipore<sup>®</sup>, Burlington, Massachusetts, USA), supernatants were recovered and analyzed for  
210 free PTM using UV absorbance at 270 nm. Calibration was performed using PTM solutions at  
211 different concentrations from 2.5 μg·mL<sup>-1</sup> to 30 μg·mL<sup>-1</sup>. From the AE values, the loading capacity  
212 (LC) of PTM-loaded NPs was calculated using the following Equations 2 and 3 respectively:

213

$$214 \quad AE(\%) = \frac{\text{Total drug} - \text{Free drug in supernatant}}{\text{Total drug}} \times 100 \quad (2)$$

$$215 \quad LC(\%) = \frac{\text{Mass of associated drug}}{\text{Mass of nanoparticles}} \times 100 \quad (3)$$

216

217 All measurements were performed in triplicate using PTM aqueous solution as control.

218

### 219 **2.9. Stability studies of blank and pentamidine-loaded nanoparticles**

220 Colloidal stability of HA-PArg NPs and PTM-loaded NPs was evaluated over 4 weeks under  
221 storage at 4 °C. Size, polydispersity index and  $\zeta$  potential were analyzed every week. Leakage of  
222 the drug was also evaluated at the end of the storage period. The stability in DMEM without  
223 glucose, glutamine, phenol red and sodium pyruvate was tested to check the effect of protein factors  
224 on NPs aggregation.

225

### 226 **2.10. *In vitro* release study of pentamidine-loaded nanoparticles**

227 *In vitro* release behavior of PTM-loaded NPs in simulated physiological conditions (PBS at 37 °C)  
228 was performed using a bicompartamental diffusion device (Franz cells) mounted with a semi-  
229 synthetic cellulose membrane (6-8 kDa MWCO from Spectra/Por, Spectrum Laboratories, The  
230 Netherlands). To ensure sink condition, 2 mL of PTM-loaded NPs prepared using 2.3 and  
231 3.3 mg·mL<sup>-1</sup> of HA and 0.50 mg·mL<sup>-1</sup> of PTM were placed in the upper part of the cell (donor  
232 chamber). The lower part of the cell (receptor chamber) was filled with 10 mL of release media  
233 (PBS, pH 7.4 at 37 °C) with an horizontal shaking. At different time points (15 min, 30 min, 1 h,  
234 2 h, 3 h, 4 h, 6 h, 8 h, 24 h, 48 h, 72 h), 1 mL of each sample was collected and analyzed for PTM  
235 using UV absorption (at 270 nm). The amount of drug released over time was calculated from the  
236 difference between the initial total amount of the drug present in PTM-loaded NPs and the amount

237 of PTM present in the receptor chamber. The experiments were performed for both NPs in  
238 triplicate.

239

### 240 **2.11. Freeze-drying studies of blank and loaded pentamidine nanoparticles**

241 Once the development of NPs has been completed, HA-PArg NPs and PTM-loaded NPs were  
242 freeze-dried using CRYONEXT pilot freeze dryer (Cryotec, Saint-Gély-du-Fesc, France). During  
243 the formulation step, the bulking agent mannitol was added to the formulations at different  
244 concentration (5%, 10% w/v). The freeze-drying program consisted of an initial freezing at -20°C in  
245 a freezer for 12 h. After that, the freeze-dryer was pre-cooled at -20°C and samples were introduced  
246 therein. Then, the temperature was decreased to -50°C at a rate of 1°C·min<sup>-1</sup> and this temperature  
247 was kept for 12 h. The sublimation step was carried out at a temperature between -35°C and 5 °C  
248 and a pressure between 0.100 and 0.3000 mbar according to the recipe. Finally, a secondary drying  
249 step was carried out at 35 °C and 0.010 mbar. After freeze-drying, HA-PArg NPs and PTM-loaded  
250 NPs were resuspended in 1 mL of milli-Q water and left under magnetic stirring for 30 min. Size,  
251 polydispersity and association efficiency of nanoparticles were measured before and after  
252 resuspension. Also, morphological observations using TEM were performed.

253

### 254 **2.12. *In vitro* cell viability studies**

255 Human lung carcinoma cells (A549) and human breast adenocarcinoma cells (MDA-MB-231) were  
256 used to evaluate the cell viability. Cells (3000 cells/well) were seeded in 96 well plates in 100 µL  
257 media and left to adhere for 24 h. Then, the medium was replaced with a fresh one containing  
258 different concentrations (0.01-100 µM) of free PTM, HA-PArg NPs and PTM-loaded NPs. After  
259 72 h of exposure, metabolically active cells were quantified by 3-(4,5-dimethylthiazol-2-yl)-2,5-  
260 diphenyltetrazolium bromide (MTT) assay according to the supplier's instructions. Briefly, 20 µL  
261 of MTT reagent (5 mg·mL<sup>-1</sup>) was added in each well and the plate was incubated at 37 °C for 2 h.  
262 After that the supernatant was replaced by 100 µL of isopropanol/HCl/H<sub>2</sub>O (90/1/9 v/v/v) and the

263 optical density was measured at 540 nm for purple intensity and at 690 nm for the subtraction of  
264 background using a multiwell-scanning spectrophotometer (Multiskan Ascent, LabSystems SA,  
265 Cergy-pontoise, France). Cell viability from the absorbance values was calculated using the  
266 following Equation 4:

$$267 \quad \text{Cell viability (\%)} = \frac{Abs_{treated}}{Abs_{untreated}} \times 100 \quad (4)$$

268 IC50 values were determined using the CompuSyn software.

269

### 270 **3. Results and discussion**

#### 271 **3.1. Solubility of pentamidine at different pH**

272 PTM isethionate is a synthetic amidine derivative, highly soluble in water ( $> 30 \text{ mg}\cdot\text{mL}^{-1}$ ) having a  
273  $pK_a$  of 12.5. Its solubility was above  $30 \text{ mg}\cdot\text{mL}^{-1}$  in the pH range from 3 to 10 due to the ionization  
274 of amidine groups, while at pH values higher than 12 the solubility was drastically reduced  
275 ( $6.5 \text{ mg}\cdot\text{mL}^{-1}$ ). Solubility also depended on ionic strength as the solubility of PTM in PBS pH 7.4  
276 was around  $6.9 \text{ mg}\cdot\text{mL}^{-1}$ . **This decrease of PTM solubility could be due to an increase of the**  
277 **concentration of inert ions in the medium that causes a salting-out effect** <sup>29</sup>.

278

#### 279 **3.2. Preparation and physicochemical characterization of pentamidine-hyaluronic acid** 280 **polyelectrolyte**

281 Polyelectrolyte complexes (PECs) are defined as complexes formed through electrostatic  
282 interactions between oppositely charged structures. The formation of PTM-HA PECs was based on  
283 the electrostatic interaction between the positively charged drug PTM containing two guanidine  
284 groups, and the negatively charged polysaccharide HA which contains one carboxylic group for  
285 each repeat unit made of two sugar residues, neutral N-acetyl-D-glucosamine and negatively  
286 charged sodium salt of D-glucuronic acid as defined in Table 1.

287 The stoichiometry of the complex was defined as the PTM/HA mole ratio of PTM molecules to HA  
 288 repeat units. Different PTM-HA PECs having a mole ratio PTM/HA between 0.2 and 2.4 and the  
 289 mass ratio from 0.24 to 3.6 (PEC A - PEC G) were obtained (Table 2). HA solution was added to an  
 290 equal volume of PTM at different concentration under magnetic stirring. Since the concentration of  
 291 the low molar mass electrolyte strongly affects the formation of the complexes, only the amount of  
 292 PTM was varied<sup>30</sup>.

293 All the formulations were prepared at pH values around 6-7 in order to obtain an optimal charge  
 294 density that generates attractive interactions between the PTM and HA.

295

296 **Table 2.** Formulation code for PTM-HA PECs. Mole ratio, mass ratio and pH values are given.

Complexes	Mole ratio PTM/HA	Mass ratio PTM/HA	pH
PEC A	0.16	0.24	7.17
PEC B	0.34	0.5	7.07
PEC C	0.67	1.0	6.78
PEC D	0.94	1.48	6.76
PEC E	1.48	2.2	6.79
PEC F	2.01	3.0	6.65
PEC G	2.42	3.6	7.17

297

298 The concentration regime of HA solutions was devised by taking measurements of overlapping  
 299 concentrations ( $C^*$ ) for aqueous solution of HA of various molar masses reported by Dodero et al.<sup>31</sup>  
 300 and extrapolating them down to the present low molar mass of HA (20 kDa). This gave  $C^* =$   
 301  $15 \text{ mg}\cdot\text{mL}^{-1}$ . The largest present HA concentration of  $2.5 \text{ mg}\cdot\text{mL}^{-1}$  was much lower than  $C^*$ ,  
 302 showing that HA concentrations were in the dilute regime.

303 DLS measurements were performed in order to study possible interactions between HA and PTM.

304 Figure 1A shows the experimental time correlation function as a function of time (at a scattering  
 305 angle of  $173^\circ$ ). For all PEC solutions, the correlation function showed a trimodal profile. This  
 306 distribution was due to the existence of fast and slow relaxation modes in molecular motions.

307 The correlation function of the scattered amplitude  $G^{(1)}(t)$  was modeled as the sum of three  
 308 exponential decays as in Equation 5 (Figure 2A):

309

$$310 \quad G^{(1)}(t) = A_1 e^{-\frac{t}{\tau_1}} + A_2 e^{-\frac{t}{\tau_2}} + A_3 e^{-\frac{t}{\tau_3}} \quad (5)$$

311

312 where  $A_i$  and  $\tau_i$  ( $i = 1, 2, 3$ ) are the relative scattered intensities and relaxation times for the three  
 313 relaxation modes respectively ( $A_1 + A_2 + A_3 = 1$ ). The first term in the right hand side of Equation 5  
 314 is the fastest relaxation corresponding to the fastest motions. It was associated with the lateral  
 315 diffusion of isolated HA-PTM complexes characterized by a mutual diffusion coefficient  $D$  ( $\tau_1^{-1} =$   
 316  $Dq^2$ ). The diameter of such species given by the Stokes-Einstein relationship ( $D = \frac{kT}{3\pi\eta \text{Diam}}$ ) was  
 317 12-14 nm (Figure 2B), in agreement with the expected size of a random coil of  $3.9 \cdot 10^4 \text{ g.mol}^{-1}$  HA.  
 318 The second term is a slower mode that was ascribed to associations (aggregates) of HA-PTM  
 319 macromolecules of mean size in the range 300-500 nm (Figure 1B). This interpretation was  
 320 suggested by observations of such aggregates in dilute solutions of HA reported by Maleki et al.<sup>32</sup>,  
 321 and in more complex systems containing HA<sup>33,34</sup>. The nature of the third mode was difficult to  
 322 figure out. The diameter of particles that would correspond to a translational diffusion was  
 323 unrealistically large ( $\sim 50 \mu\text{m}$ ) because they were not observed by optical microscopy. The origin of  
 324 this third slowest relaxation might stand from slow internal motions inside HA-PTM aggregates that  
 325 are not translational diffusion.

326

327

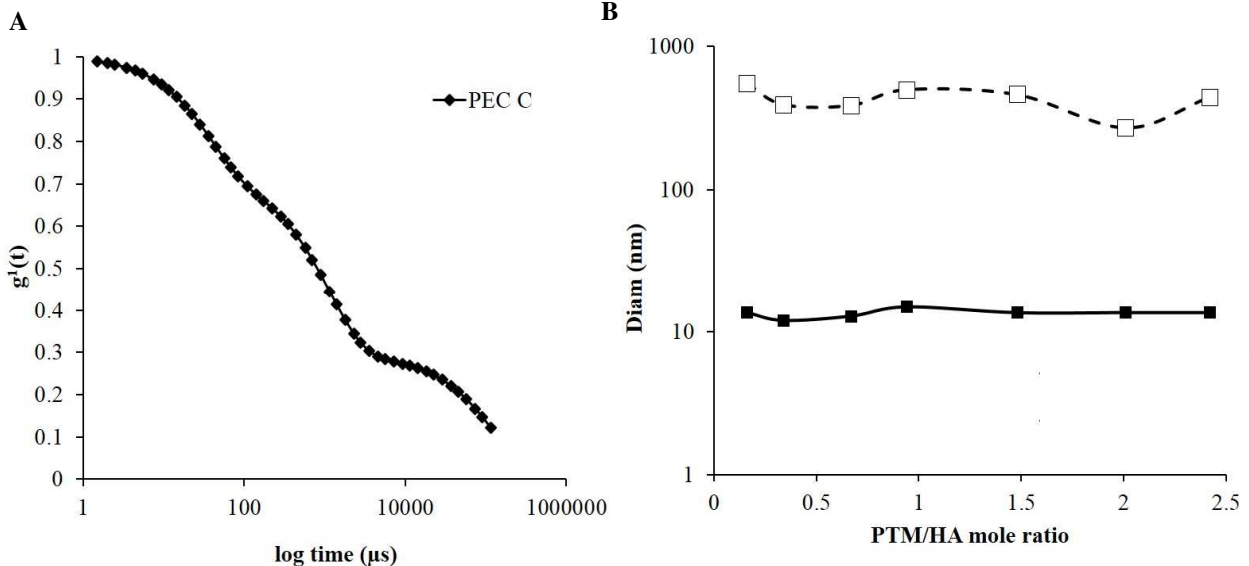
328

329

330

331

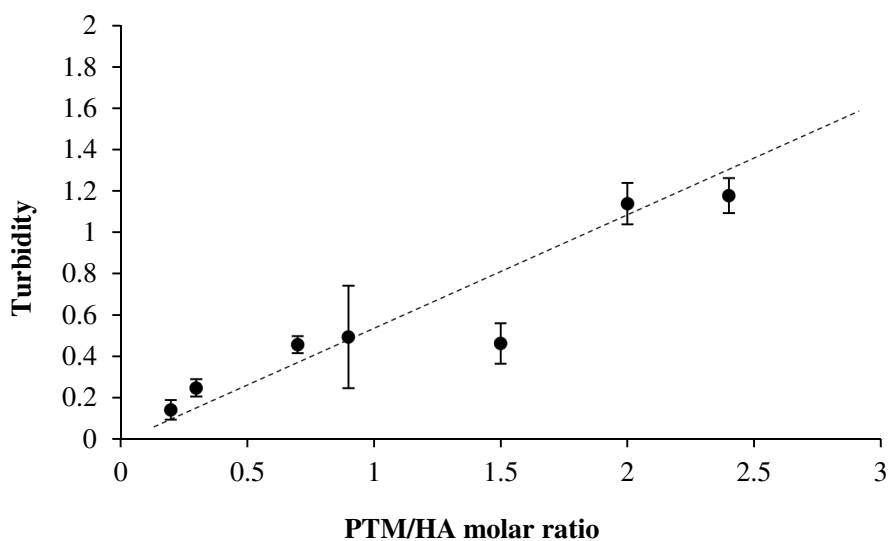
332



333 **Figure 1.** A) Normalized curve of correlation function ( $g^1(t)$ ) versus time of PECs C. The curve is  
334 fitted with the aid of the Equation 5 (see text). B) Diameter (nm) of aggregated ( $\square$ ) and isolated ( $\blacksquare$ )  
335 PEC.

336

337 Turbidity measurements of PTM-HA PECs provided a complement of the conclusions drawn from  
338 DLS (Figure 2). A slight increase of turbidity was first observed as more PTM was added to HA  
339 indicating that HA polymeric chains tended to overlap and associate each other's. As an outcome,  
340 both DLS and turbidity measurements revealed aggregation of HA as association with PTM was  
341 proceeding. The origin of such associations was probably a more hydrophobic character of the  
342 PECs as the organic PTM cations bind to HA. This provided an indirect indication for the binding  
343 of PTM to HA by means of electrostatic interaction between the two polyions.



344

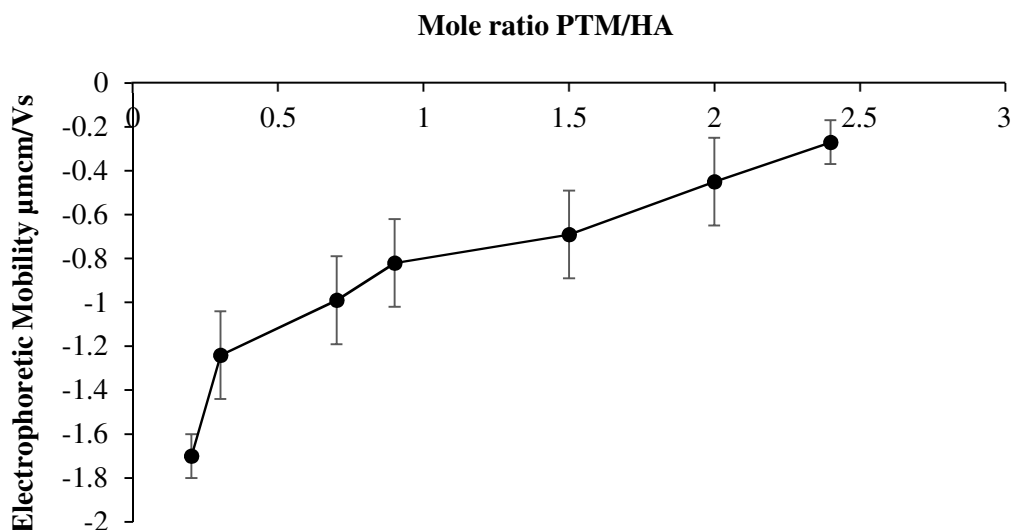
345 **Figure 2.** Turbidity ( $\lambda = 600$  nm) of PTM/HA PECs as a function of PTM/HA mole ratio. PEC A  
346 PTM/HA = 0.2, PEC B PTM/HA = 0.3, PEC C PTM/HA = 0.7, PEC D PTM/HA = 0.9, PEC E  
347 PTM/HA = 1.5, PEC F PTM/HA = 2.0, PEC G PTM/HA = 2.4. Values are given as mean  $\pm$  Sem ( $n$   
348 = 3).

349

350 Stronger binding of PTM cations than  $\text{Na}^+$  coming from the divalent and hydrophobic natures of  
351 PTM was more directly detected by measurements of electrophoretic mobility (Figure 3).



352 Electrophoretic mobility ( $u_E$ ) was negative over the whole range of PTM/HA stoichiometry,  
353 progressively shifting toward no mobility corresponding to electrical neutrality as increasing the  
354 concentration of PTM. Electrophoretic mobility experiments clearly indicated an increase of  
355 complexation at high PTM/HA mole ratio.



356  
357 **Figure 3.** Electrophoretic mobility ( $u_E$ ) of PTM-HA PECs in function of mole ratio PTM/HA (from  
358 0.24 to 2.4). Values are given as mean  $\pm$  *sem* ( $n = 3$ ).

359  
360 As an overall outcome, the conformation of the polymeric chain, turbidity and electrophoretic  
361 mobility measurements, confirmed the complexation of PTM by HA. Moreover, the electrostatic  
362 binding of PTM to HA was weak because the PTM cation was only divalent. Since the association  
363 of polyelectrolytes of opposite charges is usually quite strong, a cationic polyelectrolyte  
364 (polyarginine, PArg) was added in order to help at precipitation of nanoparticles and improve the  
365 encapsulation of PTM.

366  
367 **3.3. Preparation and physicochemical characterization of the blank hyaluronic acid-**  
368 **polyarginine nanoparticles**

369 To enhance the formation of NPs, the cationic poly(aminoacid) PArg was used as a cross-linking  
 370 agent causing the formation of insoluble PECs and thereby allowing for the formation of  
 371 nanoparticles. HA-PArg NPs were prepared by polyelectrolyte complexation in a similar manner as  
 372 described by Oyarzun-Ampuero et al.<sup>20</sup> Five hundred microliters of a solution containing HA at  
 373 different concentrations (from 1.25 to 5 mg·mL<sup>-1</sup>) were added to an aqueous solution of PArg  
 374 (0.27 mg·mL<sup>-1</sup>) under magnetic stirring at room temperature for 30 min. The formation of NPs was  
 375 ensured by the electrostatic interaction between the positively charged groups of PArg and the  
 376 negatively charged carboxylate groups of HA. All the different formulations of HA-PArg NPs  
 377 (Blank A - Blank I) were studied for their size, polydispersity index (*PdI*) and  $\zeta$  potential (Table 3).  
 378 The average size of the resulting blank NPs ranged between 112 and 244 nm with a low  
 379 polydispersity index (*PdI* < 0.2). Values of  $\zeta$  potential ranged from +33 to -22 mV. When the  
 380 charge ratio HA/PArg was lower than 1.24, NPs had a size around 120 nm with a positive  $\zeta$  value  
 381 (+33 mV), indicating that the charge brought about by PArg was larger than that of HA. At mole  
 382 ratio higher than 1.24, NPs size increased from 166 to 244 nm, and an inversion of  $\zeta$  potential to  
 383 -31 mV occurred. The increase in the hydrodynamic size was correlated to the amount of HA used  
 384 to obtain the NPs. Besides, inversion of surface potential indicated a conformational change which  
 385 exposes carboxylic groups of HA in excess with respect to cationic groups of PArg towards the  
 386 external surface of NPs. Globally, the HA/PArg interaction allows the preparation of NPs of 100-  
 387 250 nm size with a narrow size distribution and reversal of the electrical charge according to the  
 388 charge ratio of the two polymers.

389

390 **Table 3.** Physicochemical characteristics of HA-PArg NPs. *PdI*: Polydispersity index. Values are  
 391 given as mean  $\pm$  *sem* ( $n \geq 3$ ).

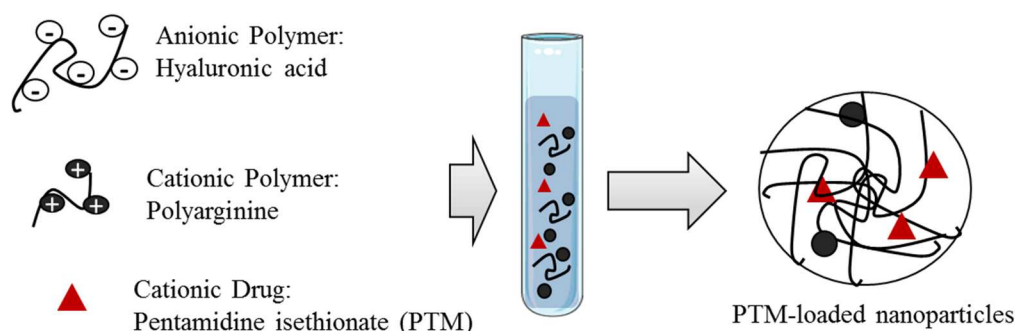
	Mass ratio [HA/PArg]	Mole ratio [HA/PArg]	Size (nm)	<i>PdI</i>	Zeta potential (mV)
Blank A	0.50: 0.27	0.82	112 $\pm$ 6	< 0.2	+ 33 $\pm$ 5

Blank B	0.75: 0.27	1.24	129 ± 1	< 0.2	+ 32 ± 3
Blank C	1.25: 0.27	2.06	166 ± 7	< 0.2	- 31 ± 1
Blank D	1.5: 0.27	2.47	158 ± 4	< 0.2	- 38 ± 2
Blank E	2.0: 0.27	3.30	167 ± 3	< 0.1	- 33 ± 2
Blank F	2.5: 0.27	4.12	180 ± 14	< 0.1	- 29 ± 3
Blank G	3: 0.27	4.95	201 ± 14	< 0.1	- 31 ± 3
Blank H	3.5: 0.27	5.77	222 ± 11	< 0.2	- 30 ± 4
Blank I	5: 0.27	8.25	244 ± 5	< 0.1	- 22 ± 3

392

### 393 3.4. Development and physicochemical characterization of pentamidine-loaded hyaluronic 394 acid-polyarginine nanoparticles

395 PTM-loaded NPs were prepared following the protocol described for blank NPs. Different  
396 concentrations of HA ( $0.83 \text{ mg}\cdot\text{mL}^{-1}$  to  $3.3 \text{ mg}\cdot\text{mL}^{-1}$ ) were added to an aqueous solution containing  
397 PArg ( $0.18 \text{ mg}\cdot\text{mL}^{-1}$ ) and PTM of concentration ranging from 0.5 to  $0.17 \text{ mg}\cdot\text{mL}^{-1}$  (Figure 4).



398

399 **Figure 4.** Preparation of PTM-loaded nanoparticles by polyelectrolyte association.

400

401 The physicochemical characterizations of NPs obtained using a PTM solution of  $0.5 \text{ mg}\cdot\text{mL}^{-1}$   
402 concentration (Table 4) showed an average size between 155 and 203 nm with a low *PdI* ( $< 0.1$ )  
403 and a negative  $\zeta$  potential ranging from -24 to -18 mV. Interestingly, the incorporation of the drug  
404 into NPs caused a reduction of NPs size compared to blank ones (Table 3). The balance between  
405 negatively (HA) and positively (PTM and PArg) charged species was reduced in the case of PTM-  
406 loaded NPs as compared to the HA-PArg NPs. Therefore, the attractive force that modulates  
407 electrostatic interactions within the complexes determined a “condensation phenomenon”

408 responsible of the reduction of the complex particle size<sup>35,36</sup>. The  $\zeta$  potential decreased from -24 to -  
 409 26 mV for Loaded A to Loaded F, and then increased to -18 mV for Loaded G. The effect of NPs  
 410 size reduction has been observed also for other particles suggesting the strong interaction between  
 411 the drug and the polymeric chains<sup>17,22</sup>.

412 Since the formation of NPs, the association of PTM to the polymers causes its encapsulation inside  
 413 the particles. Association efficiency AE is equivalent to the widely used encapsulation efficiency  
 414 EE.

415 The amounts of associated PTM varied from AE= 26% (Loaded A) to as high as AE= 82% (Loaded  
 416 G) upon increasing the HA/PArg mole ratio (Table 4). The highest encapsulation efficiencies were  
 417 obtained when the amounts of PTM were low, so that high AE (82% for Loaded G) was correlated  
 418 with low loading capacity (12% for Loaded G). Taking together all these results, PTM was  
 419 efficiently associated in HA-PArg NPs at a mole ratio above 2.25 and with a loading capacity  
 420 ranging from 20 to 10%. This data confirms that the addition of PArg to the system had the  
 421 advantageous effect of promoting the association of PTM to the systems.

422

423 **Table 4.** Physicochemical properties of PTM-loaded NPs obtained using a PTM solution at  
 424 0.5 mg·mL<sup>-1</sup>. *PdI*: polydispersity index; AE (%): association efficiency. Values are given as mean  $\pm$   
 425 *sem* ( $n \geq 3$ ).

	Mass ratio [HA: PArg: PTM]	Mole ratio [HA/PArg +PTM]	Size (nm)	<i>PdI</i>	Zeta potential (mV)	Loading capacity (%)	AE (%)
Loaded A	1.25:0.27:0.75	1.13	155 $\pm$ 3	< 0.1	-24 $\pm$ 3	33	26 $\pm$ 3
Loaded B	1.5:0.27:0.75	1.35	159 $\pm$ 4	< 0.1	-25 $\pm$ 2	30	31 $\pm$ 4
Loaded C	2:0.27:0.75	1.80	191 $\pm$ 20	< 0.1	-27 $\pm$ 2	25	46 $\pm$ 5
Loaded D	2.5:0.27:0.75	2.25	157 $\pm$ 6	< 0.1	-25 $\pm$ 5	21	61 $\pm$ 5
Loaded E	3:0.27:0.75	2.70	172 $\pm$ 14	< 0.1	-29 $\pm$ 4	19	65 $\pm$ 1
Loaded F	3.5:0.27:0.75	3.15	179 $\pm$ 4	< 0.1	-26 $\pm$ 1	17	76 $\pm$ 1
Loaded G	5:0.27:0.75	4.51	203 $\pm$ 9	< 0.1	-18 $\pm$ 1	12	82 $\pm$ 1

426

427 The fraction of associated PTM increased as a function of the concentration of HA (from Loaded A  
428 to Loaded G). The highest PTM binding efficiency was obtained for the formulation Loaded F  
429 containing  $2.3 \text{ mg}\cdot\text{mL}^{-1}$  of HA and Loaded G containing  $3.3 \text{ mg}\cdot\text{mL}^{-1}$  of HA. These results  
430 confirmed the ability of NPs to associate a high quantity of PTM by electrostatic interaction. Then,  
431 Loaded F and Loaded G were selected for the *in vitro* studies. Previous papers reported the different  
432 nanosystems for PTM encapsulation. Encapsulation of PTM inside liposome yielded an association  
433 efficiency below 50% due to the hydrophilic character of PTM<sup>37</sup>. PTM has also been encapsulated  
434 into other types polymeric NPs such as PLGA NPs. As described for the liposome formulation, the  
435 loading efficiency of PTM was very low (around 2.9%)<sup>24</sup>.  
436 Micale et al. developed PTM-HA bioconjugates in which drug loading ranged from 20 to 30%.  
437 However, the use of chemical reactions and organic solvents compromised the direct exploitation of  
438 the conjugate for drug delivery applications<sup>35</sup>.

439

### 440 **3.5. Quantification of isethionate ions using ion-exchange chromatography**

441 According to electrostatic binding of counterions to polyelectrolytes in solution, the ion  
442 concentration in the counterion cloud that surrounds the charged molecules is significantly higher  
443 than that in the solution, especially at low ionic strength. Formation of an electrostatic complex of  
444 PTM with HA weakens electrostatic binding of isethionate counterions to PTM, so, isethionate  
445 counterions are released in bulk solution. The balance is a competitive binding of HA and  
446 isethionate to PTM which is shifted towards HA because of its large negative charge (it is a  
447 polyelectrolyte) compared to the monovalent isethionate anion. In case of full ion exchange of HA  
448 for isethionate, the overall charge of the particles varies as the PTM/HA mole ratio. In the absence  
449 of ion exchange (adsorption of the neutral PTM-isethionate ion pair), loading PTM does not change  
450 electrostatic phenomena with respect to blank NPs. The balance of isethionate binding to NPs  
451 controls the NPs charge, thus the onset of NPs formation. When two opposite charged macro-ions  
452 form a complex, as in the case of HA with PTM and PArg, the electrical double layer is perturbed

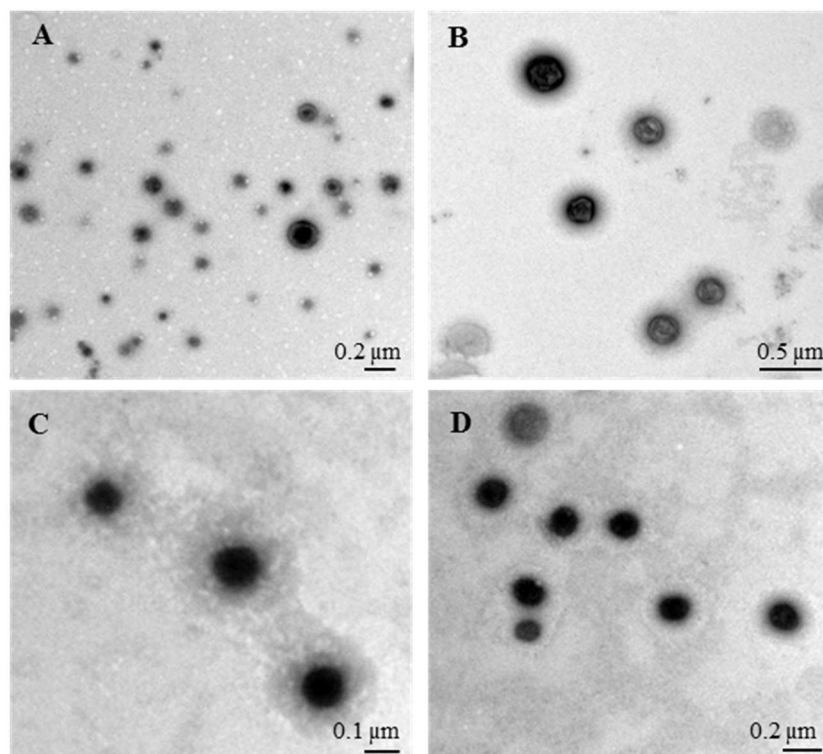
453 and counterions are released to the bulk solution<sup>38</sup>. To assess the influence of HA concentration on  
454 the formation of PTM-loaded NPs (Loaded B, C, D, E and F), the release of isethionate, the  
455 counterion of PTM, was quantified using ion exchange chromatography. The results show that the  
456 full amount of isethionate was released upon formation of all NPs irrespective of the amount of HA.  
457 This shows that electrostatic interactions between HA and PTM are predominant. It should be kept  
458 in mind that association by strong interactions remains an equilibrium that could be shifted  
459 according to changes of external condition (pH, ionic strength).

460

### 461 **3.6. Morphological analysis of blank and pentamidine-loaded nanoparticles**

462 The morphological analysis of HA-PArg NPs (Blank H and I) and PTM-loaded NPs (Loaded F and  
463 G) was carried out using TEM and Cryogenic transmission electron microscopy (CryoTEM). As  
464 shown in Figure 5, HA-PArg NPs and PTM-loaded NPs formed monodispersed population of  
465 regular rounded-shaped particles as observed by DLS measurements. The addition of the drug did  
466 not modify the morphology of the NPs.

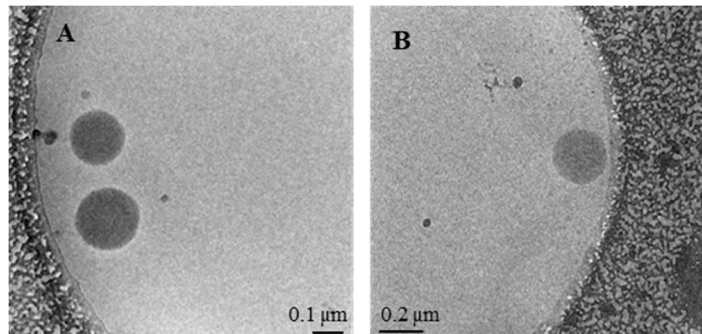
467 Besides, to prepare TEM samples, NPs were stained and dried before the analysis. This preparation  
468 step might modify the structure of the NPs. Observation NPs in their native state was achieved with  
469 Cryo-TEM. Both measurements showed similar results and confirmed the DLS analysis (Figure 6).



470

471

472 **Figure 5.** TEM images of Blank H (A); Blank I (B); Loaded F (C) and Loaded G (D).



473

474

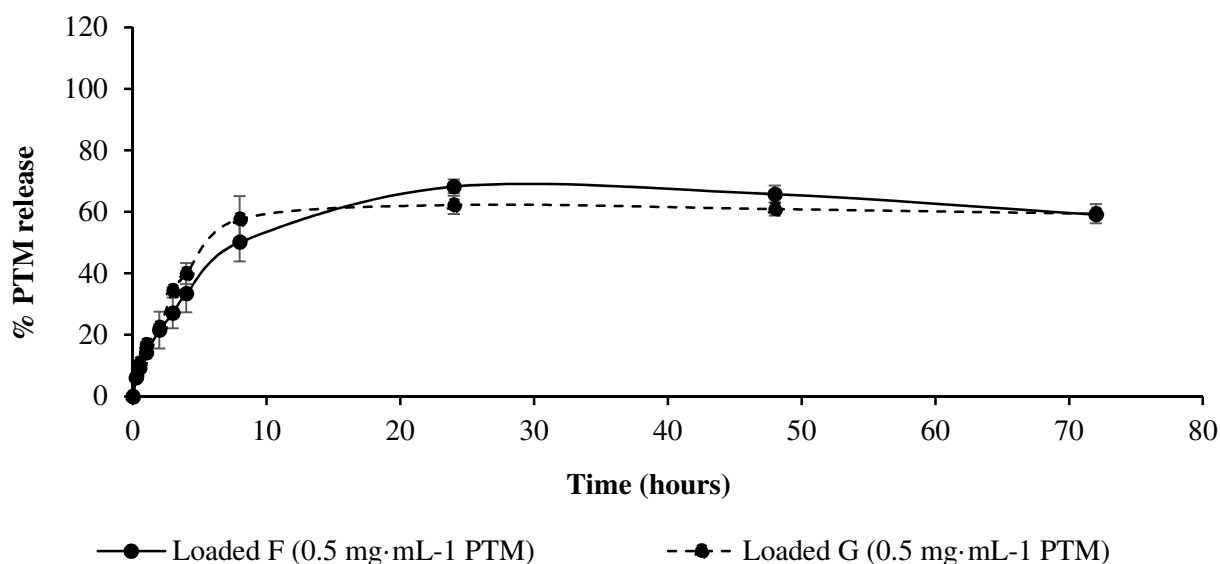
475 **Figure 6.** Cryo-TEM images of Loaded F with 2.3 mg·mL<sup>-1</sup> of HA (A) and Loaded G with  
 476 3.3 mg·mL<sup>-1</sup> of HA (B).

477

### 478 3.7. *In vitro* release study of pentamidine-loaded nanoparticles

479 The release study was performed for HA-PArg NPs (loaded F and loaded G) upon incubation with  
 480 PBS at 37°C using vertical diffusion Franz cells. For both formulations a biphasic release profile  
 481 characterized by an initial burst release in the first 8 h, 6% of release after 15 min increasing up to

482 50% after 8 h, was observed. Then, a plateau was reached and no further release was detected until  
483 72 h (Figure 7). This behavior has been described also for others hydrophilic polymer-based NPs<sup>39</sup>.  
484 According to the authors, the encapsulation of a hydrophilic drug allows a faster penetration of  
485 water in the system causing the swelling of polymeric matrix and the formation of pores. The initial  
486 burst release is probably due to a fast erosion of the surface that cause the disaggregation of the  
487 polymeric matrix with a fast drug release. When the swelling of the matrix is compensated by  
488 erosion process a constant release towards water as receptor medium was observed. Moreover, the  
489 release behavior of PTM from NPs was similar to the control PTM solution. This shows that the  
490 rate-limiting step of the experiment was the diffusion of PTM through the dialysis membrane.



491  
492 **Figure 7.** Release profile of PTM from loaded F and loaded G in PBS medium. The diffusion cells were  
493 thermoregulated with water at 37°C circulating in a double jacket. (Mean  $\pm$  Sem.; n = 3).  
494

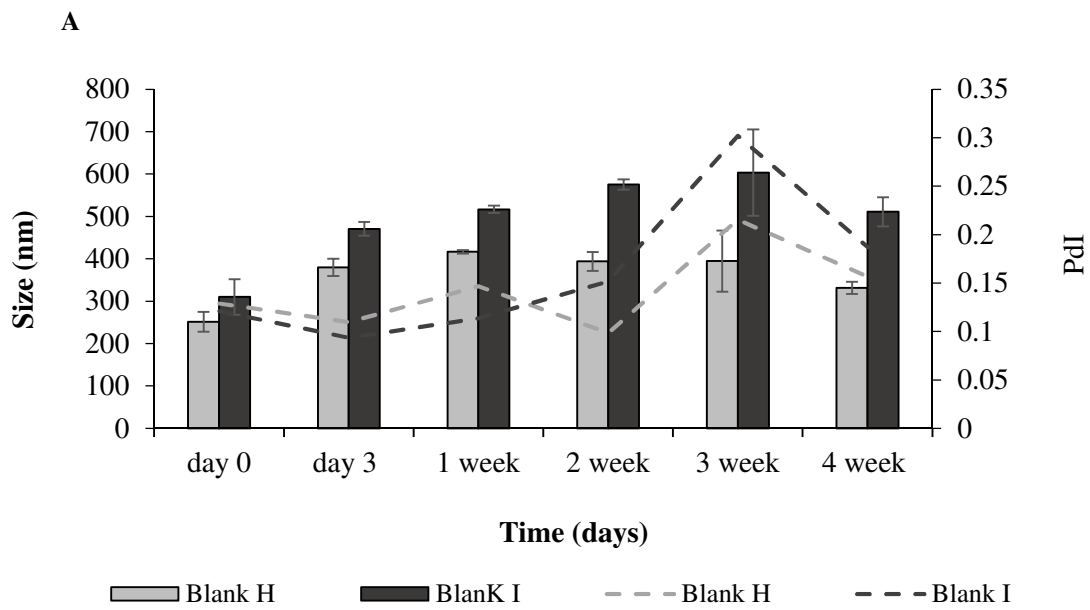
### 495 3.8. Stability studies of blank and pentamidine-loaded nanoparticles

496 The stability of colloidal suspensions of Blank H and I (Figure 8-A) and Loaded F and G (Figure 8-  
497 B) NPs at 4 °C was evaluated over 1 month of storage. Size, polydispersity index and leakage of  
498 PTM were evaluated every week. As reported in Figure 8-A and B, size and *Pdl* of Blank H and I  
499 increased over time for both formulations. However, Blank (H-I) and Loaded NPs (F-G) were more

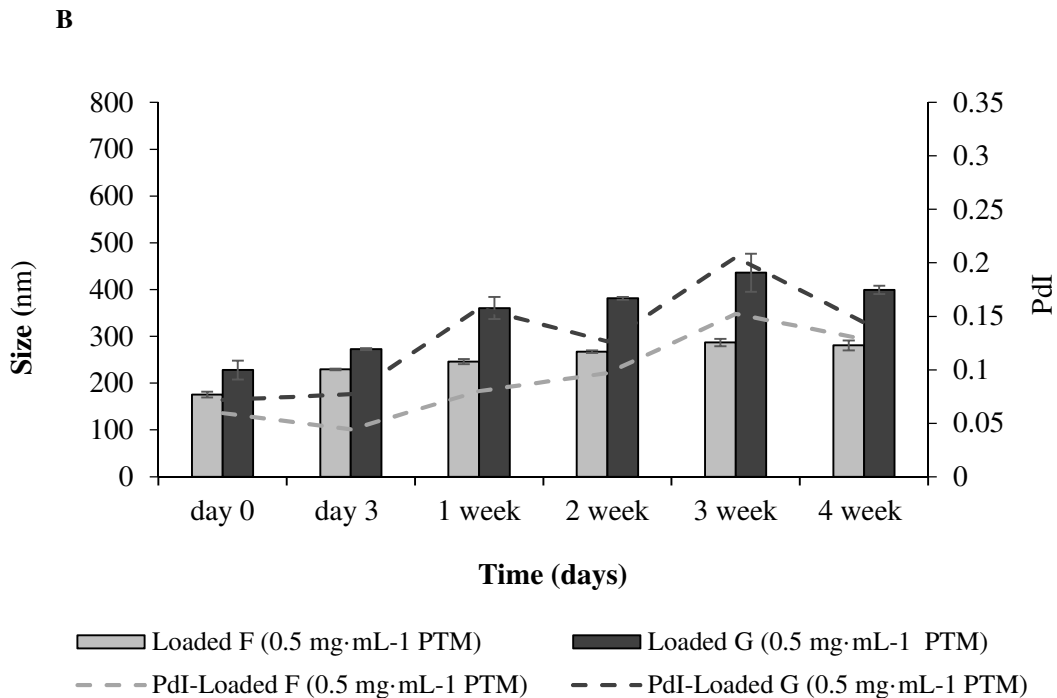


500 stable cause they were more negative and more stabilized by electrostatic repulsions. No leakage of  
 501 the drug was observed for both formulations, demonstrating the ability of NPs to associate PTM in  
 502 an efficient manner. In addition, Blank H and PTM-Loaded F did not aggregate in DMEM (data not  
 503 shown).

504



505



506

507 **Figure 8.** Stability studies, size and *PdI*, upon storage condition for 4 weeks at 4°C in aqueous  
 508 solution of Blank H (3.5 mg·mL<sup>-1</sup> of HA), Blank I (5 mg·mL<sup>-1</sup> of HA) (A) and Loaded F

509 (2.3 mg·mL<sup>-1</sup> of HA), Loaded G (3.3 mg·mL<sup>-1</sup> of HA) (B). *PdI*: polydispersity index. (Mean ± *sem*;  
510 *n* = 3).

511

### 512 3.9. Freeze-drying studies of blank and pentamidine-loaded nanoparticles

513 A dry form of blank and loaded NPs selected was prepared by freeze-drying in order to study the  
514 long-term stability. The optimal freeze-drying conditions that convert the aqueous suspension into  
515 dry powder and allow for reconstitution in physiological medium were set up. Blank H, Blank I,  
516 Loaded F and Loaded G were freeze-dried using different amount of mannitol (5%, 10% w/v) as  
517 bulking and isotonic agent. The aim was to obtain isotonic values close to physiological condition  
518 (280-300 mOsm·L<sup>-1</sup>). Tables 5 and 6 show the physicochemical characteristics (size, *PdI* and  
519 osmolarity) of Blank H and Loaded F formulations prepared with different mannitol concentrations,  
520 before and after redispersion in water. Also, stability after redispersion was evaluated over 15 days  
521 at 4 °C. Blank H and Loaded F, were successfully dispersed in water irrespective of the amount of  
522 mannitol used. However, 5% mannitol was needed to obtain isotonic formulation. Following  
523 reconstitution in water, the size of HA-PArg NPs and PTM-loaded NPs increased. Moreover, the  
524 size continued to increase during the storage period for the both formulations (Table 5-6). However,  
525 the population remained monodispersed (*PdI* > 0.1) and no leakage of the drug during the time was  
526 observed. **Figure 9** confirms that both Blank H and Loaded F recovered the initial morphology  
527 characteristics upon freeze-drying and reconstitution in water. Both formulations formed  
528 monodispersed population showing a regular round shape and no aggregation was detected.

529

530 **Table 5.** Physicochemical characterization of Blank H before and after freeze-drying and  
531 reconstitution. *PdI*: polydispersity index. Results are expressed as mean values ± *sem*; *n* = 3.

5% mannitol				10% mannitol		
Days	Size (nm)	<i>PdI</i>	Osmol. (mOsm·L <sup>-1</sup> )	Size (nm)	<i>PdI</i>	Osmol. (mOsm·L <sup>-1</sup> )

0	151 ± 5	< 0.1	-	148 ± 6	-	-
0	218 ± 5	< 0.1	665	210 ± 8	< 0.1	305
8	233 ± 7	< 0.1	665	254 ± 11	< 0.2	305
16	315 ± 45	< 0.1	665	383 ± 42	< 0.2	305

532

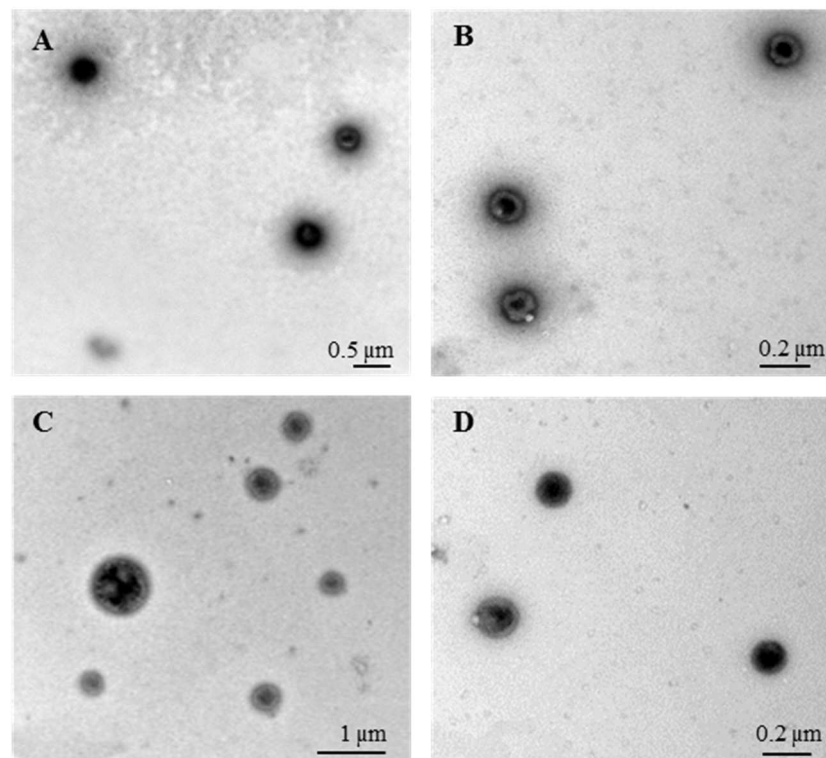
533 **Table 6.** Physicochemical characterization of Loaded F after freeze-drying and reconstitution. *PdI*:

534 polydispersity index. *AE (%)* association efficiency. Results are expressed as mean values ± *sem*; *n*

535 = 3.

5% mannitol					10% mannitol			
Days	Size (nm)	<i>PdI</i>	<i>AE (%)</i>	Osmol. (mOsm·L <sup>-1</sup> )	Size (nm)	<i>PdI</i>	<i>AE (%)</i>	Osmol. (mOsm·L <sup>-1</sup> )
0	149 ± 1	< 0.1	79 ± 1	-	157 ± 6	-	64 ± 2	-
0	234 ± 12	< 0.2	76 ± 1	669	204 ± 12	< 0.1	64 ± 4	297
8	287 ± 13	< 0.1	-	669	265 ± 3	< 0.1	-	297
16	353 ± 6	< 0.1	78 ± 1	669	321 ± 10	< 0.2	75 ± 1	297

536



537

538

539 **Figure 9.** TEM pictures of Blank H (A-B) and Loaded F (C-D) nanoparticles after freeze-drying

540 and reconstitution in 1 mL of water.

### 541 **3.10. *In vitro* cell viability studies of pentamidine-loaded nanoparticles**

542 The antiproliferative activity of free and encapsulated PTM into Loaded F was assessed using the  
543 MTT assay. Lung (A549) and human breast cancer (MDA-MB-231) cell lines were selected based  
544 on their sensitivity to PTM<sup>23,40</sup>. The viability of A549 and MDA-MB-231 was monitored after  
545 incubation with different concentrations of free PTM and PTM-loaded NPs for 72 h. Blank H were  
546 used as controls to evaluate the biocompatibility of the nanocarrier. As shown in Table 7, the use of  
547 Loaded F was associated with a better activity than free PTM both on lung (IC<sub>50</sub> = 0.21 ± 0.08 μM  
548 vs 1.2 ± 0.8 μM) and breast cancer cells (IC<sub>50</sub> = 2.2 ± 1.8 μM vs 4.6 ± 3.7 μM). Blank I showed  
549 very low toxicity (IC<sub>50</sub> > 40 μM) highlighting the biocompatibility of the nanocarrier. These data  
550 confirmed that PTM activity *in vitro* was improved when the drug was incorporated inside  
551 nanoparticles.

552 As reported in the literature both cell lines express CD44 receptors<sup>41,42</sup>. Hence, we suggest that the  
553 present NPs can target cancer cells *in vivo* through interaction with this receptor.

554 In line with our study, Battistini et al.<sup>16</sup> observed that in A549 cells, cytotoxicity of HA-doxorubicin  
555 complexes was 3-fold higher than that of the reference free drug. These results indicated an  
556 increased cellular uptake of doxorubicin when complexed with HA due to the presence of CD44  
557 membrane receptors<sup>14</sup>. Targeting CD44 using HA moieties has also been demonstrated *in vivo* in  
558 CD44-positive human breast tumor xenografts mice. HA based micelles loaded with paclitaxel  
559 exhibit a remarkably high accumulation and retention in the CD44 receptor-overexpressing tumor  
560 following intravenous injection in comparison to the free drug<sup>15</sup>.

561

562 **Table 7.** IC<sub>50</sub> values of studied compounds on A549 and MDA-MB-231 cells. Results are  
563 expressed as mean values ± *sem*; *n* = 3.

Cell line	Formulations	IC <sub>50</sub> (μM)
	PTM	1.2 ± 0.8

A549	PTM-loaded NPs	0.21 ± 0.08
	Blank HA NPs	42 ± 16
MDA-MB-231	PTM	4.6 ± 3.7
	PTM-loaded NPs	2.2 ± 1.8
	Blank HA NPs	66 ± 47

564

565

#### 4. Conclusions

566

567

568

569

570

571

572

573

574

575

576

577

578

579

580

The present study provides insight into a new HA based nano-complex, namely nanoparticles, for encapsulation of positively charged hydrophilic drug. In a first set of experiments, HA-PTM complexes were studied. Such complexes were highly polydispersed species that remained soluble in water. To stabilize the complex and to maximize the amount of the drug associated to the system, HA-PArg NPs were developed using polyelectrolyte complexation technique. NPs were kinetically stabilized by the excess charge, which prevented their aggregation and ensured high encapsulation efficiency of PTM. Also, high encapsulation efficiency was associated to the release of the isethionate counterion in the solution quantified by IC. Following *in vitro* studies, PTM-loaded NPs were more effective in reducing cell viability as compared with free drug suggesting enhanced efficacy and cell internalization via CD44 receptor. Moreover, their optimum pharmaceutical properties, namely easy production using mild conditions, stability and possibility to obtain ready-to-use dry powders, highlight the potential of HA-PArg nanoparticles as novel drug delivery system for nanomedicine applications.

#### Funding Sources

581

582

583

584

This work has been carried out within the research program RESOLVE, financially supported by EuroNanoMed-III (8<sup>th</sup> call). Flavia Carton had a fellowship from the Ministry of Education of Italy. The research leading to these results has received funding from Italian Ministry for University and Research (MIUR)-University of Torino, “Fondi Ricerca Locale (ex-60%)”.

585

586 **Notes**

587 The authors declare no competing financial interests.

588

589 **Acknowledgements**

590 Authors are thankful to Geraldine Agusti, Sébastien Urbaniak from University of Lyon 1, CNRS,  
591 LAGEPP UMR 5007, for their kind help with TEM images and lyophilization studies. We would  
592 like to acknowledge the contribution of Pierre-Yves Dugas (University of Lyon 1, C2P2 UMR  
593 5265) for cryo-TEM observations at the “Centre Technologique des Microstructures” (CT $\mu$  -  
594 University of Lyon 1). Emeline Perrial and Zineb Bousfiha from CRCL, are gratefully  
595 acknowledged for cell culture.

596 **References**

- 597 1. Marras A, Vieregg J, Ting J, Rubien J, Tirrell M. Polyelectrolyte Complexation of  
598 Oligonucleotides by Charged Hydrophobic – Neutral Hydrophilic Block Polymers.  
599 *Polymers*. 2019;11,83.
- 600 2. Myung GK, Sung DJ, Ji HJ, Sun HK. Nanoscale polyelectrolyte complexes encapsulating  
601 mRNA and long-chained siRNA for combinatorial cancer gene therapy. *J Ind and end chem*.  
602 2018;64:430-437.
- 603 3. Joshi JR, Patel RP. Role of biodegradable polymers in drug delivery. *Int J Curr Pharm Res*.  
604 2012;4:74-81.
- 605 4. Goycoolea FM, Lollo G, Remuñán-López C, Quaglia F, Alonso MJ. Chitosan-alginate  
606 blended nanoparticles as carriers for the transmucosal delivery of macromolecules.  
607 *Biomacromolecules*. 2009;10:1736-1743.
- 608 5. Pistone S, Goycoolea FM, Young A, Smistad G, Hiorth M. Formulation of polysaccharide-  
609 based nanoparticles for local administration into the oral cavity. *Eur J Pharm Sci*.  
610 2017;96:381-389.
- 611 6. Weber C, Drogoz A, David L, Domard A, Charles MH, Verrier B, Delair T. Polysaccharide-  
612 based vaccine delivery systems: Macromolecular assembly, interactions with antigen  
613 presenting cells, and in vivo immunomonitoring. *J Biomed Mater Res - Part A*.  
614 2010;93:1322-1334.
- 615 7. Liu Z, Jiao Y, Wang Y, Zhou C, Zhang Z. Polysaccharides-based nanoparticles as drug  
616 delivery systems. *Adv Drug Deliv Rev*. 2008;60:1650-1662.
- 617 8. Morra M. Engineering of biomaterials surfaces by hyaluronan. *Biomacromolecules*.  
618 2005;6:1205-1223.

- 619 9. Dosio F, Arpicco S, Stella B, Fattal E. Hyaluronic acid for anticancer drug and nucleic acid  
620 delivery. *Adv Drug Deliv Rev.* 2016;97:204-236.
- 621 10. Chen B, Miller RJ, Dhal PK. Hyaluronic acid-based drug conjugates: State-of-the-art and  
622 perspectives. *J Biomed Nanotechnol.* 2014;10:4-16.
- 623 11. Cadete A. Targeting cancer with hyaluronic acid-based nanocarriers: recent advances and  
624 translational perspectives. *Nanomedicine.* 2016;11:2341-2357.
- 625 12. Lee GY, Kim J-H, Choi KY, Yoon HY, Kim K, Kwon IC, Choi K, Lee B-H, Park JH, Kim I-  
626 S. Hyaluronic acid nanoparticles for active targeting atherosclerosis. *Biomaterials.*  
627 2015;53:341-348.
- 628 13. Fallacara A, Baldini E, Manfredini S, Vertuani S, Hyaluronic Acid in the Third Millennium.  
629 *Polymers.* 2018;10(7):701.
- 630 14. Battistini FD, Flores-Martin J, Olivera ME, Genti-Raimondi S, Manzo RH. Hyaluronan as  
631 drug carrier. The in vitro efficacy and selectivity of Hyaluronan-Doxorubicin complexes to  
632 affect the viability of overexpressing CD44 receptor cells. *Eur J Pharm Sci.* 2014;65:122-  
633 129.
- 634 15. Zhong Y, Goltsche K, Cheng L, Xie F, Meng F, Deng C, Zhong Z, Haag R. Hyaluronic acid-  
635 shelled acid-activatable paclitaxel prodrug micelles effectively target and treat CD44-  
636 overexpressing human breast tumor xenografts in vivo. *Biomaterials.* 2016;84:250-261.
- 637 16. Battistini FD, Olivera ME, Manzo RH. Equilibrium and release properties of hyaluronic  
638 acid-drug complexes. *Eur J Pharm Sci.* 2013;49:588-594.
- 639 17. Thomas RG, Moon MJ, Lee SJ, Jeong YY. Paclitaxel loaded hyaluronic acid nanoparticles  
640 for targeted cancer therapy: In vitro and in vivo analysis. *Int J Biol Macromol.* 2014;72:510-  
641 518.



- 642 18. Choi KY, Chung H, Min KH, Yoon HY, Kim K, Park JH, Kwon IC, Jeong SY. Self-  
643 assembled hyaluronic acid nanoparticles for active tumor targeting. *Biomaterials*.  
644 2010;31:106-114.
- 645 19. Lin C, Kim SB, Yon J-M, Park SG, Gwon LW, Lee J-G, Baek I-J, Lee BJ, Yun YW, Nam S-  
646 Y. Temporal and subcellular distributions of Cy5.5-labeled hyaluronic acid nanoparticles in  
647 mouse organs during 28 days as a drug carrier. *Korean J Vet Res*. 2017;57:215-222.
- 648 20. Oyarzun-Ampuero FA, Goycoolea FM, Torres D, Alonso MJ. A new drug nanocarrier  
649 consisting of polyarginine and hyaluronic acid. *Eur J Pharm Biopharm*. 2011;79:54-57.
- 650 21. Contreras-Ruiz L, de la Fuente M, Párraga JE, López-García A, Fernández I, Seijo B,  
651 Sánchez A, Calonge M, Diebold Y. Intracellular trafficking of hyaluronic acid-chitosan  
652 oligomer-based nanoparticles in cultured human ocular surface cells. *Mol Vis*. 2011;17:279-  
653 290.
- 654 22. Lollo G, Benoit JP, Brachet M, Drug delivery system, European Patent Office  
655 (EP18306201.7)2018, Pending licence.
- 656 23. Jung HJ, Suh S Il, Suh MH, Baek WK, Park JW. Pentamidine reduces expression of  
657 hypoxia-inducible factor-1 $\alpha$  in DU145 and MDA-MB-231 cancer cells. *Cancer Lett*.  
658 2011;303:39-46.
- 659 24. Arias JL, Unciti-Broceta JD, Maceira J, del Castillo T, Hernández-Quero J, Magez S,  
660 Soriano M, García-Salcedo JA. Nanobody conjugated PLGA nanoparticles for active  
661 targeting of African Trypanosomiasis. *J Control Release*. 2015;197:190-198.
- 662 25. Lollo G, Gonzalez-Paredes A, Garcia-Fuentes M, Calvo P, Torres D, Alonso MJ.  
663 Polyarginine nanocapsules as a potential oral peptide delivery carrier. *J Pharm Sci*.  
664 2017;106:611-618.

- 665 26. Wang S, Cao M, Deng X, Xiao X, Yin Z, Hu Q, Zhou Z, Zhang F, Zhang R, Wu Y, Sheng  
666 W, Zeng Y. Degradable hyaluronic acid/protamine sulfate interpolyelectrolyte complexes as  
667 miRNA-delivery nanocapsules for triple-negative breast cancer therapy. *Adv Healthc Mater.*  
668 2015;4:281-90.
- 669 27. González-Aramundiz JV, Peleteiro Olmedo M, González-Fernández Á, Alonso Fernández  
670 MJ, Csaba NS.. Protamine-based nanoparticles as new antigen delivery systems. *Eur J Pharm*  
671 *Biopharm.* 2015;97(Pt A):51-9
- 672 28. R. J. Hunter, *Zeta Potential in Colloid Science. Principles and Applications*, Academic Press,  
673 London, 1981.
- 674 29. Long FA and McDevit HM. Activity coefficients of nonelectrolyte solutes in aqueous salt  
675 solutions. *Chem Rev.* 1952;51:119-169.
- 676 30. Dautzenberg H. Polyelectrolyte complex formation in highly aggregating systems. 1. Effect  
677 of salt: Polyelectrolyte complex formation in the presence of NaCl. *Macromolecules.*  
678 1997;30:7810-7815.
- 679 31. Doderò A, Williams R, Gagliardi S, Vicini S, Alloisio M, Castellano M. Characterization of  
680 hyaluronic acid by dynamic light scattering and rheological techniques. *AIP Conf Proc.*  
681 2018;1981:020184-1-020184-4.
- 682 32. Maleki A, Kjøniksen AL, Nyström B. Effect of pH on the behavior of hyaluronic acid in  
683 dilute and semidilute aqueous solutions. *Macromol Symp.* 2008;274:131-140.
- 684 33. Nyström B, Lindman B. Dynamic and viscoelastic properties during the thermal gelation  
685 process of a nonionic cellulose ether dissolved in water in the presence of ionic surfactants.  
686 *Macromolecules.* 1995;28(4):967-974.
- 687 34. Maleki A, Kjøniksen AL, Knudsen KD, Nyström B. Dynamical and structural behavior of

- 688 hydroxyethylcellulose hydrogels obtained by chemical gelation. *Polym Int.* 2006;55:365.
- 689 35. Micale N, Piperno A, Mahfoudh N, Schurigt U, Schultheis M, Mineo PG, Schirmeister T,  
690 Scala A, Grassi G. A hyaluronic acid-pentamidine bioconjugate as a macrophage mediated  
691 drug targeting delivery system for the treatment of leishmaniasis. *RSC Adv.* 2015;5:95545-  
692 95550.
- 693 36. Paul M, Durand R, Boulard Y, Fusai T, Fernandez C, Rivollet D, Deniau M, Astier A.  
694 Physicochemical characteristics of pentamidine-loaded polymethacrylate nanoparticles:  
695 Implication in the intracellular drug release in *Leishmania major* infected mice. *J Drug*  
696 *Target.* 1998;5:481-490.
- 697 37. Mérian J, De Souza R, Dou Y, Ekdawi SN, Ravenelle F, Allen C. Development of a liposome  
698 formulation for improved biodistribution and tumor accumulation of pentamidine for  
699 oncology applications. *Int J Pharm.* 2015;488:154-164.
- 700 38. Van der Guch J, Spruijt E, Lemmers M, Coen Stuart MA. Polyelectrolyte complexes: Bulk  
701 phases and colloidal systems, *J Colloid Interface Sci.* 2011;361:407-422.
- 702 39. Chakraborty S1, Khandai M, Sharma A, Patra ChN, Patro VJ, Sen KK. Effects of drug  
703 solubility on the release kinetics of water soluble and insoluble drugs from HPMC based  
704 matrix formulations. *Acta Pharm.* 2009; 59:313-323.
- 705 40. Lee MS, Johansen L, Zhang Y, Wilson A, Keegan M, Avery W, Elliott P, Borisy AA, Keith  
706 CT. The novel combination of chlorpromazine and pentamidine exerts synergistic  
707 antiproliferative effects through dual mitotic action. *Cancer Res.* 2007;67:11359-11368.
- 708 41. Olsson E, Honeth G, Bendahl PO, Saal LH, Gruvberger-Saal S, Ringnér M, Vallon-  
709 Christersson J, Jönsson G, Holm K, Lövgren K, Fernö M, Grabau D, Borg A, Hegardt C.  
710 CD44 isoforms are heterogeneously expressed in breast cancer and correlate with tumor  
711 subtypes and cancer stem cell markers. *BMC Cancer.* 2011;11:418.

712 42. Jeannot V, Mazzaferro S, Lavaud J, Vanwonderghem L, Henry M, Arboléas M, Vollaire J,  
713 Jossierand V, Coll JL, Lecommandoux S, Schatz C, Hurbin A. Targeting CD44 receptor-  
714 positive lung tumors using polysaccharide-based nanocarriers: Influence of nanoparticle size  
715 and administration route. *Nanomedicine*. 2016; 12(4):921-932.

Anionic polymer  
Hyaluronic acid



Cationic polymer  
Polyarginine

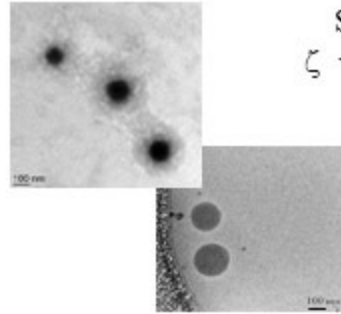


Pentamidine  
isethionate (PTM)



### Physico-chemical characterization

TEM and Cryo-TEM

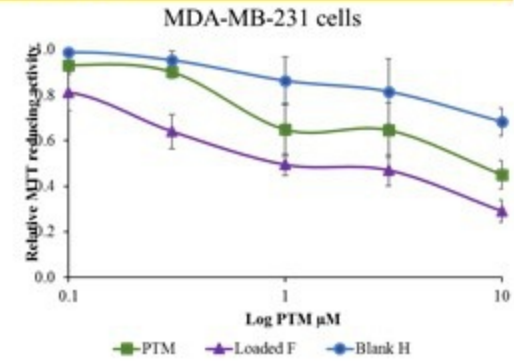
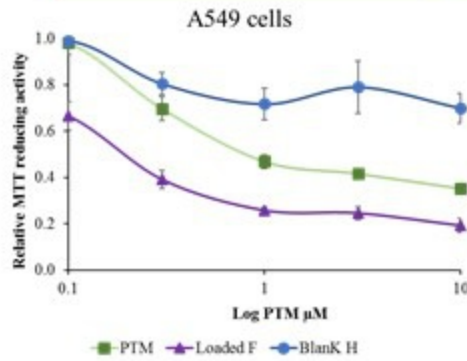


Size from 155 to 203 nm  
 $\zeta$  values from -24 to -18 mV  
Low PdI (<0.1)

Freeze-drying



### Citotoxicity assay



PTM-loaded NPs induced a significant reduction in cell viability in comparison with PTM solution.